FINAL REPORT

IN-SITU ION IRRADIATION TO ADD IRRADIATION ASSISTED GRAIN GROWTH TO THE MARMOT TOOL

Award Number.....17-12797

Project Begin Date .....October 1, 2017
Project End Date.....December 31, 2021
Project Quarter 17

Principal Investigator ...Arthur Motta
atm2@psu.edu
The Pennsylvania State University

Co-PI: Michael Tonks, University of Florida
Co-PI: Zefeng Yu, Penn State, Chris Ulmer (Penn State)
With the participation of Dr. Aiping Chen (LANL) and Wei-Ying Chen (ANL)

Abstract

In the Nuclear Energy Advanced Modeling and Simulation (NEAMS) program, the MARMOT mesoscale fuel performance tool is used to inform the development of mechanistic materials models for the BISON fuel performance tool. The grain size of the fuel has a large impact on its performance, directly impacting heat conduction, fission gas release, creep, and fracture. Thus, atomistic and mesoscale MARMOT simulations have been used to investigate grain boundary migration and grain growth in UO_2. However, the current grain growth models in MARMOT does not consider the effect of irradiation on causing grain growth. This research project experimentally studied and implemented irradiation effects on grain growth of UO_2 into MARMOT.

Summary Table of Tasks Performed

Milestone	Task	Progress	Projected Completion Date
1	Prepare nano-grained UO_2 TEM samples	100%	Y2
2	Characterize UO_2 microstructure	100%	Y2
3	In-situ isothermal annealing grain growth experiments of UO_2	100%	Y3
4	MARMOT simulation of isothermal annealing grain growth	100%	Y3
5	In-situ isothermal irradiation grain growth experiments of UO_2	100%	Y3
6	MARMOT simulation of isothermal irradiation grain growth	100%	Y3
7	Prepare nano-grained CeO_2 TEM samples	100%	Y2
8	Characterize CeO_2 microstructure	100%	Y2
9	In-situ TEM grain growth of CeO_2	100%	Y3

Publications and Presentations

1. C.J. Ulmer, W-Y. Chen, D.E. Wolfe, A.T. Motta, "In-situ ion irradiation induced grain growth in nanocrystalline ceria", *Journal of Nuclear Materials*, Volume 545 (2021) 152688, ISSN 0022-3115.
2. Zefeng Yu, Xinyuan Xu, Wei-Ying Chen, Yogesh Sharma, Xing Wang, Aiping Chen, Christopher J. Ulmer, Arthur T. Motta, In-situ irradiation-induced studies of grain growth kinetics of nanocrystalline UO_2, submitted to Acta Materialia, November 2021.
3. Zefeng Yu, Arthur T. Motta, Wei-Ying Chen, Aiping Chen, Xinyuan Xu, Xin Wang, Christopher J. Ulmer, "In-situ grain growth of nanocrystalline UO_2", to be presented at the TMS 2022 Annual Meeting, March 2022.
4. Md Ali Muntaha, Larry Aagesen, Michael Tonks, Zefeng Yu, Arthur Motta, "Adding irradiation-assisted grain growth to the MARMOT tool for UO_2 nuclear fuel," to be presented at the TMS 2022 Annual Meeting, March 2022.
5. Wei-Ying Chen, Rajat Sainju, Zhi-Gang Mei, Gai Hao, Zefeng Yu, Samuel Schaefer, Yuanyuan Zhu, Logan Ward, Abdelatif Yacout, Gady Agam, Arthur Motta, Meimei Li, "Computer Vision Application for in-situ Transmission Electron Microscopy of Irradiation Process," to be presented at the TMS 2022 Annual Meeting, March 2022.

Tasks Performed

1. Preparation of CeO_2 and UO_2 thin films through physical vapor deposition onto TEM grids/substrates. This was done at Penn State (CeO2) and Los Alamos (UO2).
2. In situ irradiation of the prepared thin films at the Intermediate Voltage Electron Microscope (IVEM) at Argonne National Laboratory, at a range of temperatures. Thermal annealing of the same samples in the IVEM.. Both of these tasks generated a series of micrographs showing grain growth.
3. The TEM micrographs went through detailed analysis using both a manual method and machine learning, to determine the average grain diameter as a function of dose for each temperature and as a function to time for straight annealing experiments.
4. The analytical model developed by Kaoumi et al[1] was used to interpret the data to yield a formula that describes the grain growth kinetics as a function of ion dose and temperature.
5. Irradiation-induced grain growth was implemented into MARMOT by coupling a heat conduction model with the phase field grain growth model and introducing heat generation in regions the size of displacement cascades at random locations and times. This resulted high temperature spikes allowing for atomic jumps that caused grain growth. The results were benchmarked with the experimental results.

Conclusions

The main conclusions are:

1. The irradiation-induced grain growth in UO_2 was measured and modeled and implemented into MARMOT. The in-situ method is an effective way to measure and follow grain growth both with and without irradiation.
2. The main effect of irradiation induced grain growth from thermal spikes occurs at temperatures below 400 C. Above this temperature the thermal effects start to dominate the grain growth process.

Education/Training

Two post-doctoral researchers – Drs. Chris Ulmer and Zefeng Yu were educated in this project, working at Penn State. Dr, Ulmer has now taken a job with the NRC while Dr. Yu has joined U.S. Steel. A PhD student M. Ali Muntaha, at the University of Florida worked on the phase field implementation of the model.

Irradiation campaign on UO_2 at the IVEM

In the early part of the project CeO_2 was irradiated, to serve as a test for UO_2. The ceria samples were prepared by Doug Wolfe at Penn State. The UO_2 thin films samples were prepared by Dr. Aiping Chen at Los Alamos National Laboratory and sent to Dr. Wei-Ying Chen at Argonne National Laboratory. These samples were thin UO_2 films deposited on grids which allowed for multiple irradiations to be conducted.

The samples were irradiated with 1 MeV Kr ions at a count rate of 6.25×10^{12} ion/cm^2/s which corresponds to a total of over 10^{15} ions/cm^2/s for the irradiation times used, at seven temperatures: 50 K, 300 K, 375 K, 475 K, 675 K, 875 K and 1073 K. The samples were characterized by systematically taking bright-field and dark-field images during irradiation as well as diffraction patterns.

[1] Kaoumi, D., A. T. Motta, and R. C. Birtcher, "A Thermal Spike Model of Grain Growth under Irradiation," *Journal of Applied Physics*, 104 (2008) 073525

Completed Irradiation Matrix:

Sample Name	Irradiation temperature (K)	Fluence (KC)
1st sample	50	0,16,80,160,240,320,480,640,800,1120
2th sample	50	0,16,80,160,240,320,480,640,800,1120
3rd sample	300	0,16,80,160,240,320,480,640,800,1120
4th sample	300	0,16,80,160,240,320,480,640,800,1120
5th sample	375	0,16,34,64,94,130,200,400,600,800
6th sample	475	0,16,34,64,94,150,200,400,600,800,1000
7h sample	475	0,16,32,64,100,200,300,500,700,900
8th sample	675	0,16,80,160,240,320,480,640,800,1120
9th sample	675	0,16,80,160,240,340,480,640,800
10th sample	875	0,30,60,100,300,600,800,1000
11th sample	1075	0,16,80,160,240,320,480,640
12th sample	1075	0,16,32,64,120,300,600,800,1000
13th sample	1075	0,16,32,64,100,200,400,600,800

Note: 1KC (kilocounts) ≈ 6.36 x 10 ^{16} (ions/m^2).

In-situ isothermal annealing experiments were been done on samples without irradiation. The annealing temperatures were 200, 400, 600 and 800 °C for up to 5 hours.

Summary of grain growth of in-situ irradiated UO_2 at various temperatures

The TEM images in Figure 1 to Figure 7 illustrate the observed grain growth of UO_2 thin films at various irradiation temperatures. At each temperature, grain size has consistently increased at the highest dose relative to the as-synthesized sample. It is important to point out that thermally assisted grain growth becomes increasingly stronger as the temperature increases. The threshold temperature for significant thermal effect seems to be close to 475 K.

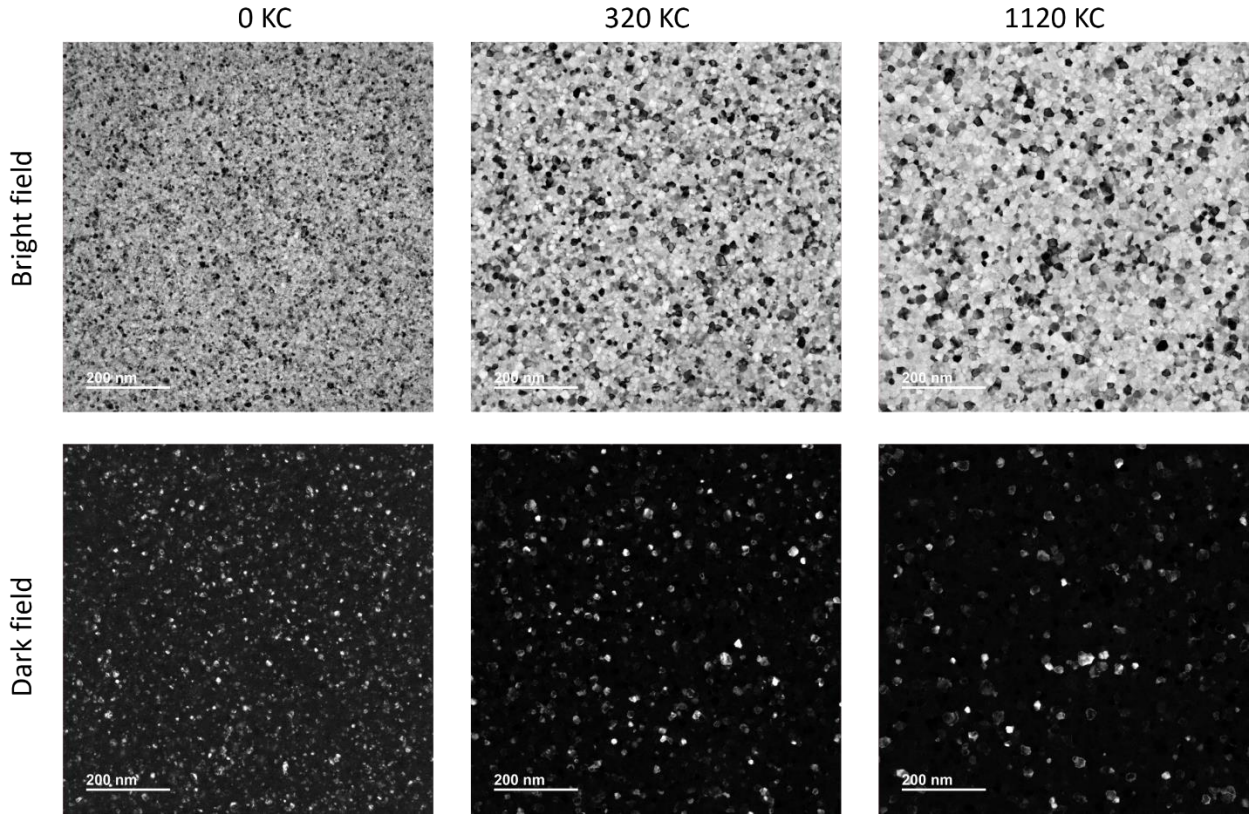

Figure 1. Bright field (BF) and Dark-field (DF) images of unirradiated and irradiated UO_2 thin film at 50K irradiation temperature.

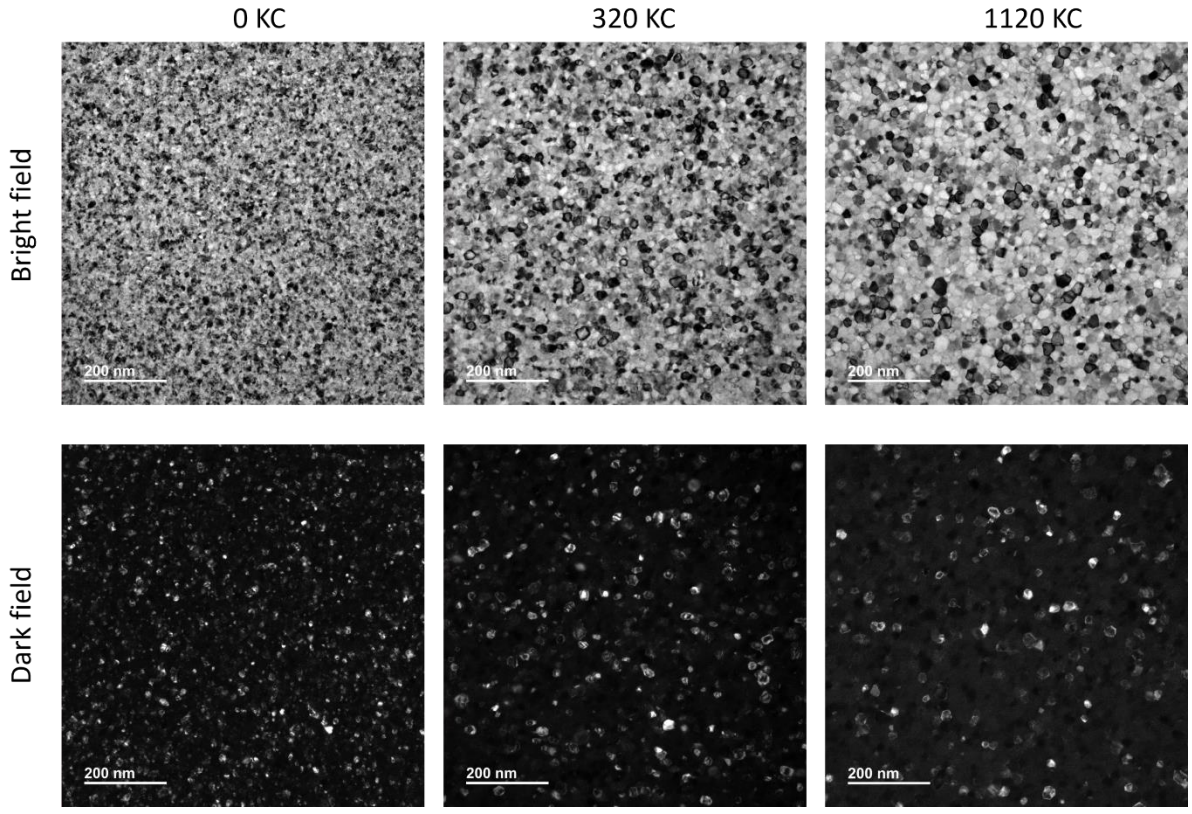

Figure 2. BF and DF images of unirradiated and irradiated UO_2 thin film at 300 K irradiation temperature.

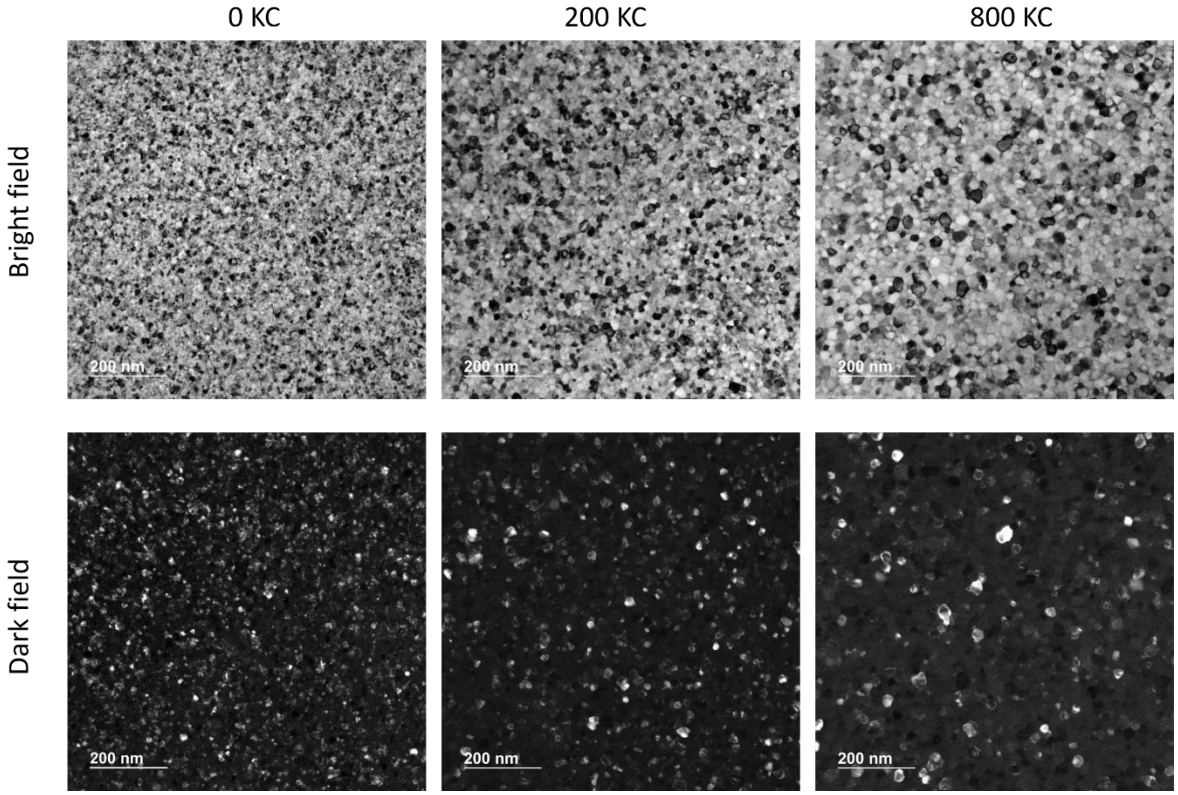

Figure 3. BF and DF images of unirradiated and irradiated UO_2 thin film at 375 K irradiation temperature.

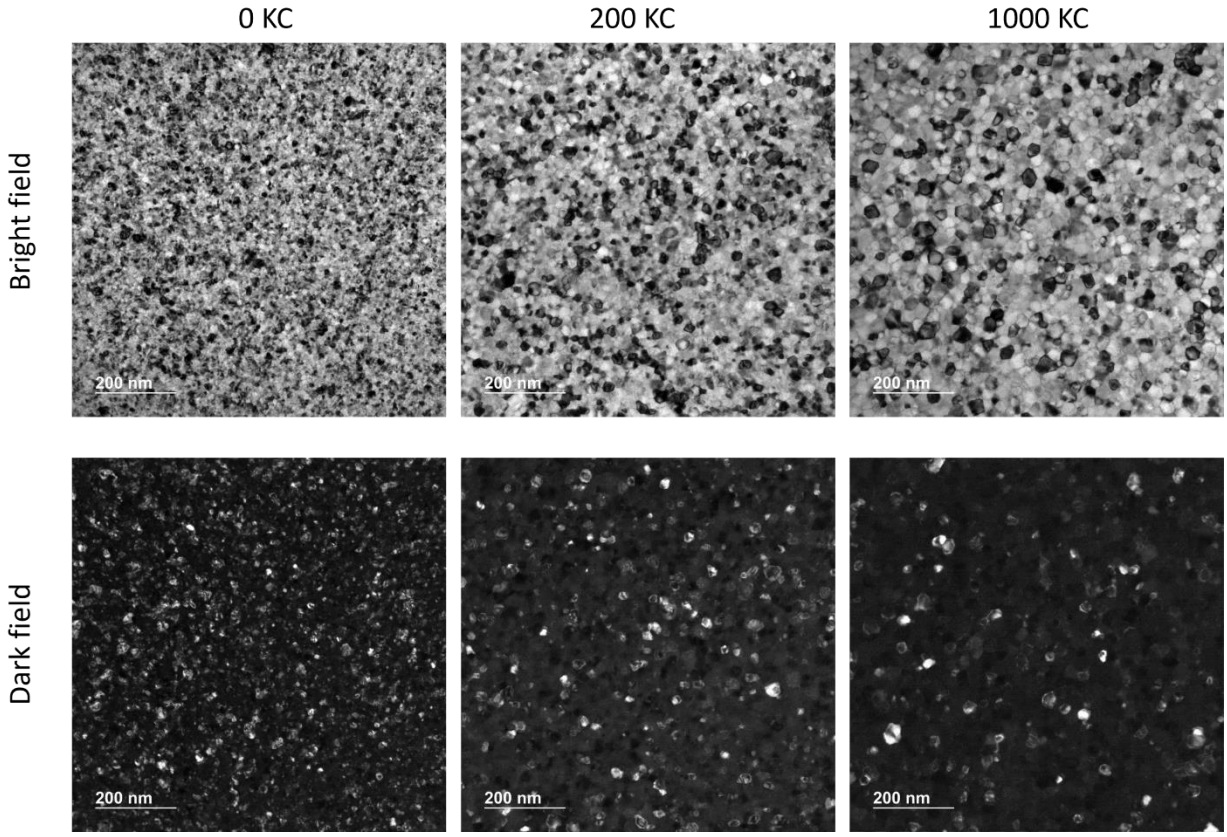

Figure 4. BF and DF images of unirradiated and irradiated UO_2 thin film at 475 K irradiation temperature.

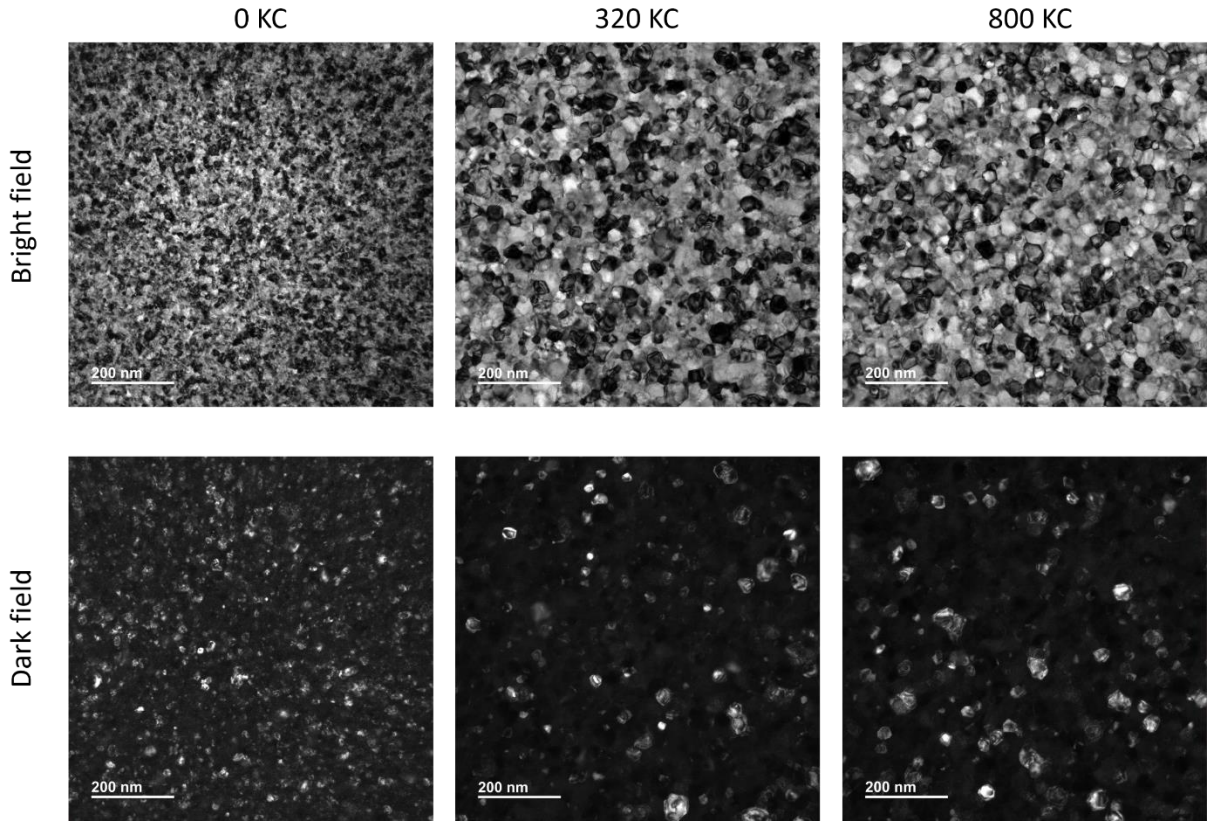

Figure 5. BF and DF images of unirradiated and irradiated UO_2 thin film at 675 K irradiation temperature.

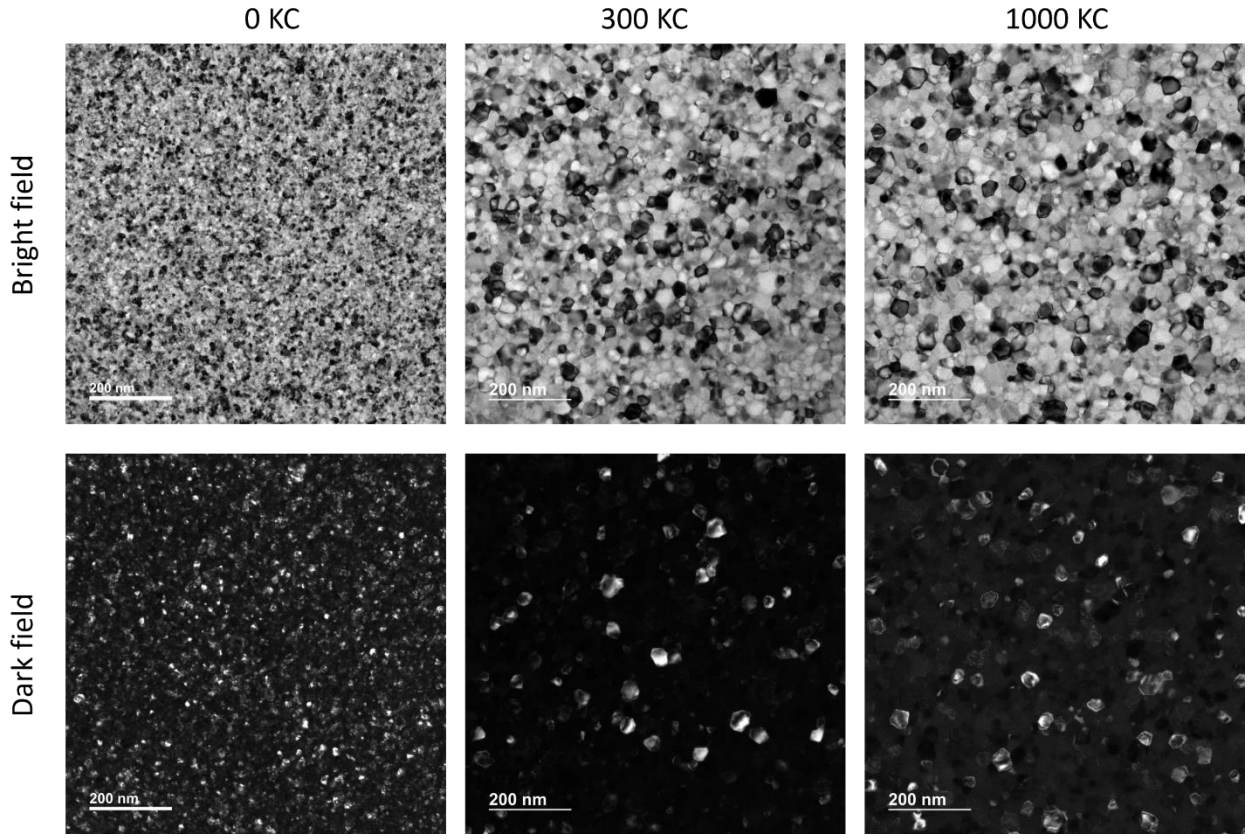

Figure 6. BF and DF images of unirradiated and irradiated UO_2 thin film at 875 K irradiation temperature.

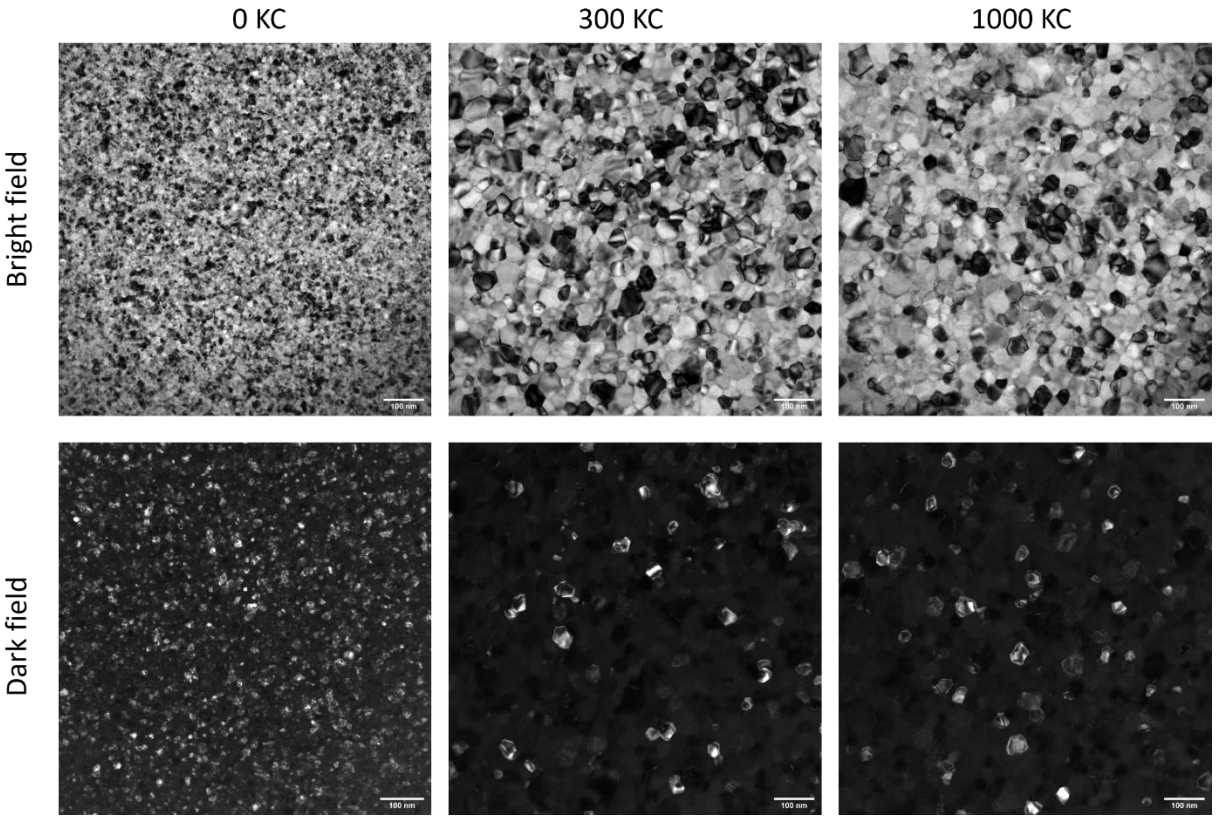

Figure 7. BF and DF images of unirradiated and irradiated UO_2 thin film at 1075 K irradiation temperature.

Data analysis by manual method

At each fluence, both bright field (BF) and dark field (DF) TEM images were taken at the same location on each sample. Taking the 4th sample irradiated at 50K as an example, Figure 8 A) shows the diffraction ring patterns of the sample at 1120KC (1KC ≈ 6.3E16 fluence (ions/m^2)). Figure 8 B) shows the BF images at 100kX magnification and the corresponding DF images taken at the same location using either diffraction ring 1 or ring 3 at both 50kX and 100kX magnification. TEM images at these imaging conditions were used for grain diameter measurements at various fluences.

Two methods were attempted to measure the grain diameters as a function of fluence. One is the manual method, which each individual grain was identified and measured by human eye using the ImageJ program. Figure 8 C) shows the grain diameters measured by the manual method from using 100kX BF images. For each grain, two perpendicular axes were drawn and their averaged values were used to calculate the average UO_2 grain diameter at each fluence. The summarized results of the 4th sample irradiated at 50K is shown in Figure 9 A). The error bar is the standard deviation of the measured values, and it represents the large spread of the grain diameters. The grain diameter distribution is better presented in Figure 9 B) by plotting the histogram. The number of grains shown in DF image at 100kX is significantly less than in the 100kX BF and 50kX DF images. Therefore, the 100kX BF and 50kX DF images were considered to provide better statistics and higher measuring confidence. In this case, the distribution follows the normal distribution and the grain diameters with the highest counts is quite close to the average grain diameters. In addition, all the imaging condition gave similar grain size distribution. However, as will be shown later for other samples, this is not always the case.

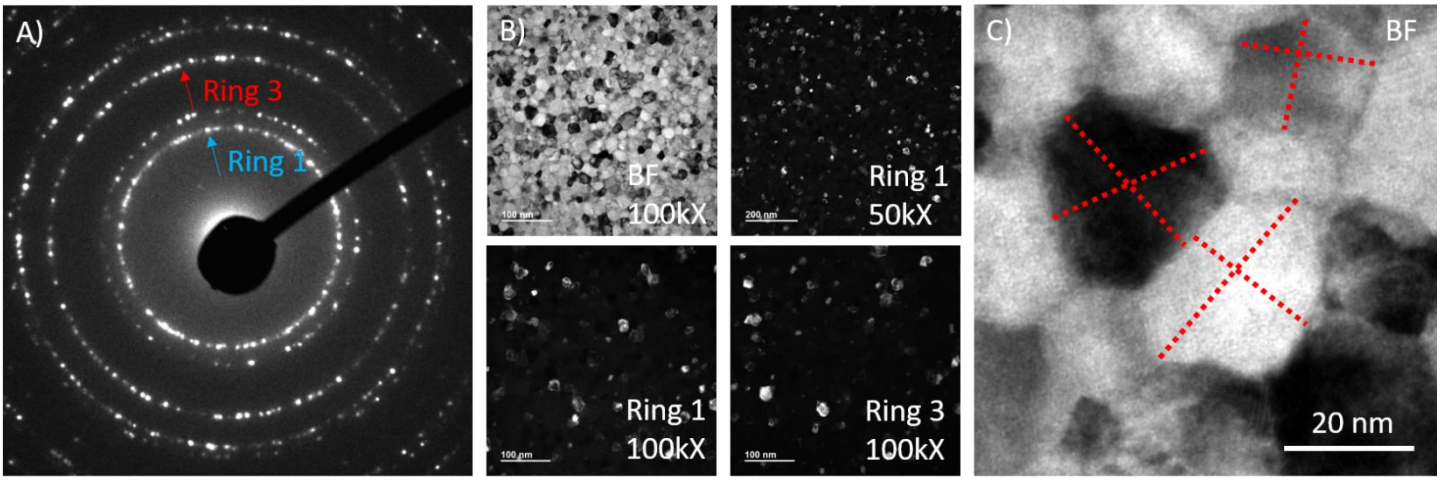

Figure 8. A) Diffraction ring patterns of irradiated UO_2 at 1120KC. 1KC ≈ 6.3E16 fluence (ions/m^2). B) TEM images of irradiated nanocrystalline UO_2 grains at 1120KC under both bright field (BF) and dark field (DF) conditions. C) Schematic showing the manual method of measuring the grain diameters on BF image. The red dash lines represent some of the measured grain diameters.

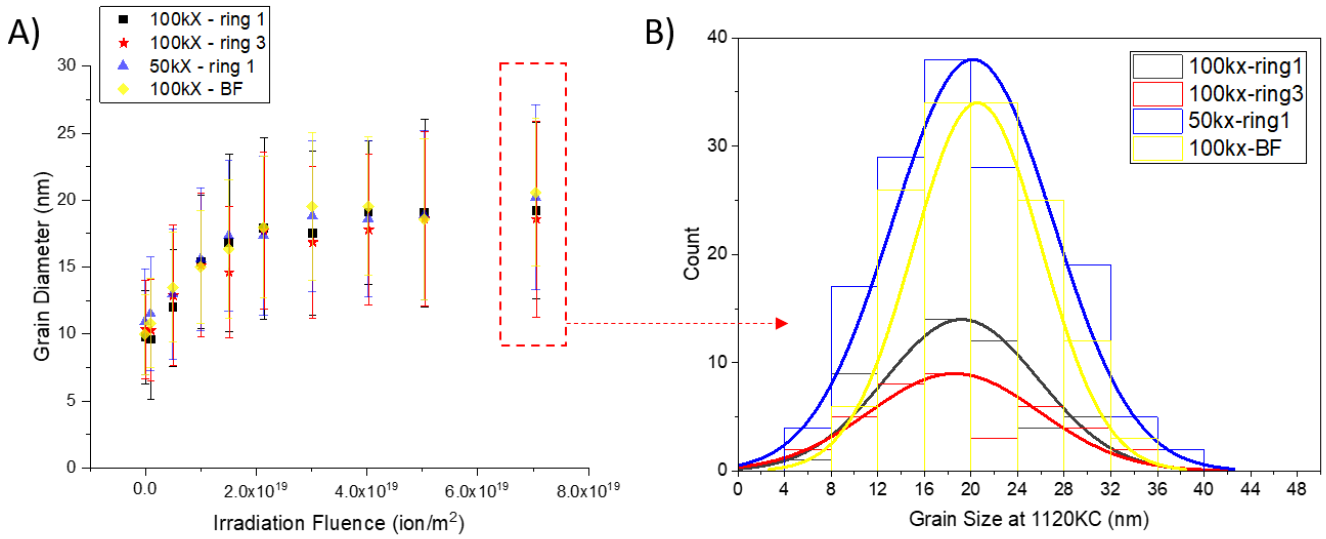

Figure 9. A) Grain diameters measured of 4th sample irradiated at 50K as a function of fluence. The error bar is the standard deviation of the measured diameters. B) Comparison of the grain diameter distribution analyzed using different imaging condition and magnification. The solid lines represent the normal distribution by fitting the data into gaussian function.

Data analysis by machine learning

The major measurement in this project is grain diameter measurement by manual (M) and machine learning (ML) methods. The M measurements were performed on both dark field (DF) and bright field (BF) TEM images at different magnifications to improve the statistics. ML measurements were only performed on 50kX DF TEM images. The machine learning method utilizes U-Net architecture, which has a unique U-shaped architecture with a contracting path to extract image context and a symmetric expansive path to propagate context information to higher resolution layers. NVIDIA Tesla P100 GPU was used to train the model to 200 epochs with L2 Regularization. The training was terminated when the validation loss became stable. The total training time was about six hours. Figure 10 compares the grain diameters measured by M and ML methods, respectively. These two methods result in great consistency. The grain diameter evolution as a function of irradiation fluence at 50 K is also plotted in Figure 10 D). There is clear grain growth at 50 K irradiation, a temperature at which there is no thermally driven grain growth processes. Therefore, the grain growth observed here is purely driven by irradiation.

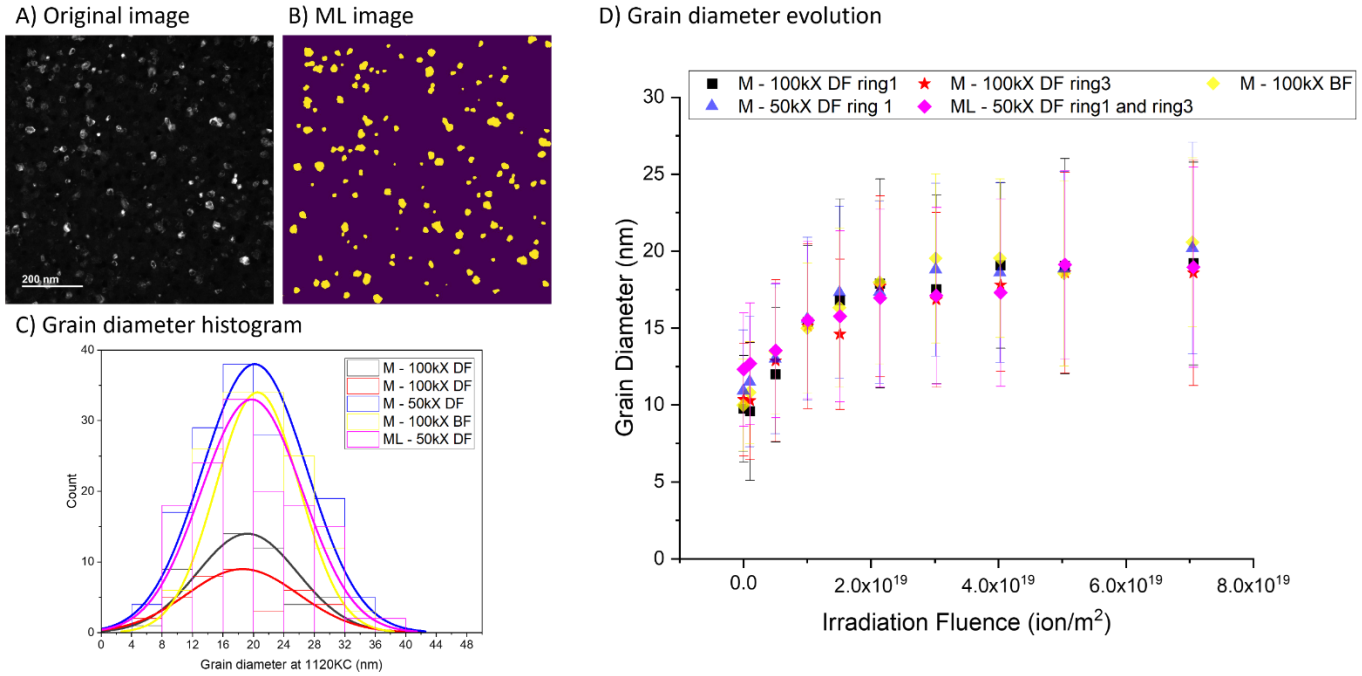

Figure 10. A) Original 50xK DF TEM image showing the grain (in white contrast) of 50 K irradiated sample. B) ML generated image showing the identified grains in yellow. C) Comparison of grain diameter measurements and distribution for both M and ML method. 1KC ≈ 6.3E16 fluence (ions/m^2). D) Grain diameter evolution plot as a function of irradiation fluence. The errors are the standard deviation of measured grain diameters.

Qualitative analysis

Quantitative analysis on the grain growth kinetics was plotted in Figure 11 A). The grain growth under 675 K and 1075 K irradiation contains thermally assisted process, which is no longer a pure irradiation effect. The data at 50 K and 475 K are fitted to a grain growth equation based on thermal spike model [3]. The fitting equation is as following

$$D^3 - D_0^3 = K\phi t \qquad (1)$$

$$K = \frac{36\gamma d_{spike} X \delta V_{at} v \sqrt{\frac{3}{5}}\Gamma\left(\frac{8}{3}\right) k_B^{\frac{5}{3}}}{10\pi C_0^{2/3} k_0} \frac{Q^{5/3}}{\left(E_a^{spike}\right)^{8/3}} \qquad (2)$$

where D_0 is the initial grain diameter, ϕ is the ion flux (ions/m^2/s), t is time (s), and K is the growth rate (nm^3/(ions/m^2)), which are obtained from fitting the measured grain diameters into eq. 1. Other variables are described in Table 1. From eq. 2, Ea can be calculated and shown in Figure 11 B) at two different temperatures. At 50 K, the Ea is about 2.5 eV, whereas it is about 1.5 eV at 475 K. However, Ea should be a temperature independent parameter. If data at 675 K and 1075 K are fitted to eq. 1 and eq. 2, the calculated Ea at higher irradiation temperatures will be even smaller. It is important to point out that eq. 2 is only valid for low temperature irradiation, where there is no thermally assisted grain growth.

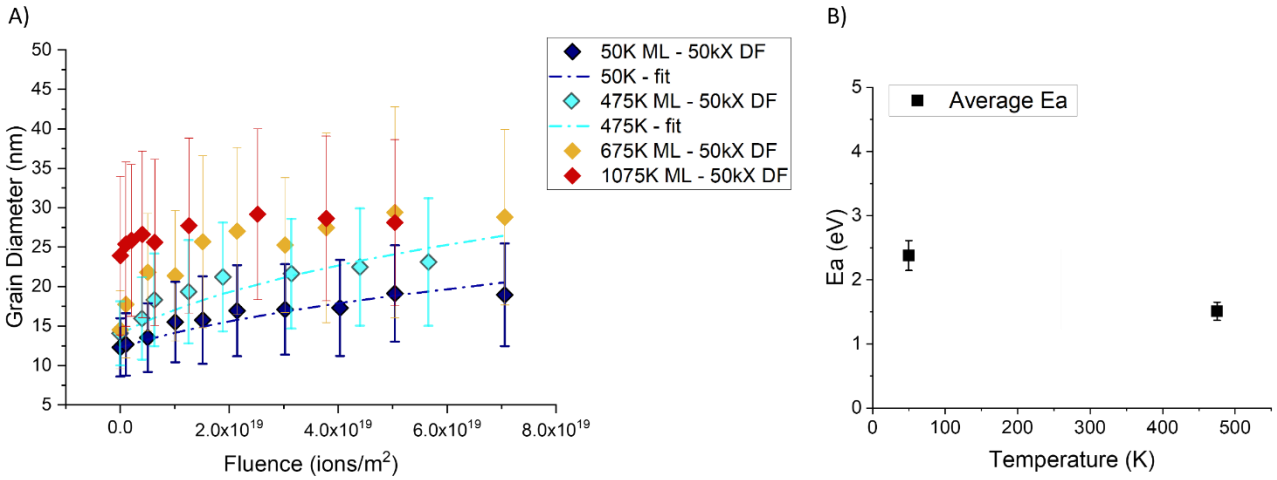

Figure 11. A) Grain diameter evolution plot as a function of irradiation fluence at different irradiation temperatures. The errors are the standard deviation of measured grain diameters. B) Calculated activation energy (E_a) for grain growth at 50K and 475 K, respectively.

Table 1. The description and literature values of the variables needed to calculate the thermal spike grain growth kinetic parameter K [6-31].

Parameters	Variables	Values
grain boundary surface energy	γ	1 (J/m^2)
thermal spike diameter	d_{spike}	9.63 (nm)
thermal spikes per ion	X	0.0407 (spikes/ion/nm)
grain boundary width	δ	0.6 (nm)
atomic volume	V_{at}	0.0136 (nm^3/atm)
Debye frequency	ν	2.20 (THz)
Boltzmann constant	k_B	8.62×10^{-5} (eV/K)
average thermal spike energy	Q	25.27 keV
heat capacity	C_0	213.96 (J/mol/K)
thermal conductivity	k_0	3 (W/m K)

To evaluate the thermal effect on the grain growth, isothermal annealing experiment without irradiation was also performed at IVEM. Both M and ML results are plotted in Figure 12. Only the annealing temperature higher than 475K would lead to grain growth. It also shows the grain growth starts to plateau

after about 2 hours annealing. These data are fitted to two different thermal grain growth equations as following

$$D^n - D_0^n = Mt \quad (3)$$

$$\frac{dD}{dt} = A\left(\frac{1}{D} - \frac{1}{D_{max}}\right) \quad (4)$$

where D is the measured grain diameter, D_0 is the initial grain diameter, n is growth rate, M is a parameter describing the grain boundary mobility, t is the annealing time, D_{max} is the measured maximum grain diameter and A is a fitted parameter similar to M. For eq. 3, n has to be greater than 10 in order to capture the plateau region. Eq. 4 with the extra resistive force can capture the plateau region perfect. By using the parameters described in [10] to obtain the A parameter, the activation energy (Q) for thermal grain growth is calculated to be 2.45 eV, which is consistent to our previously calculated E_a based on the thermal spike model.

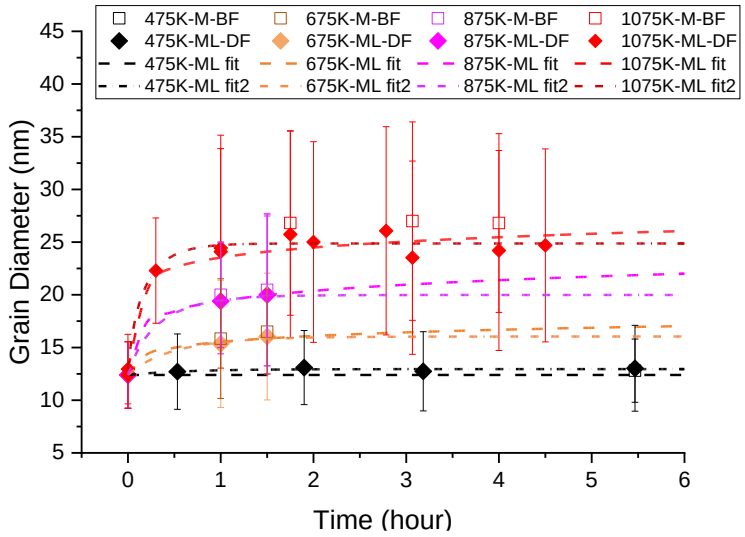

Figure 12. Grain diameter evolution under isothermal annealing.

Phase field method

The phase field method predicts microstructure evolution using continuous field variables [10, 11]. The field variables can be either conserved variables like concentration, which must remain conserved all the time, or non-conserved like order parameters, which change continuously throughout the simulation study. All the field variables are continuous across the entire domain, so there are no sharp changes in their values across the domain. Consequently, the interfaces of the microstructure are diffuse. It allows us to study the evolution of microstructures by simply solving partial differential equations even though in reality, the interfaces are really thin or sharp.

For grain growth simulation, we use order parameter variables to represents different grains and their evolution is defined by Allen-Cahn equations:

$$\frac{\partial \eta_{mj}}{\partial t} = -L_m \frac{\delta F}{\delta \eta_{mj}}.$$

Here, η_{mj} is the order parameter and the value of order parameter is 1 inside of a specific grain and zero in all other grains or orientation (Figure 13). The value of the order parameter value smoothly varies from zero to 1 over the interface or grain boundary.

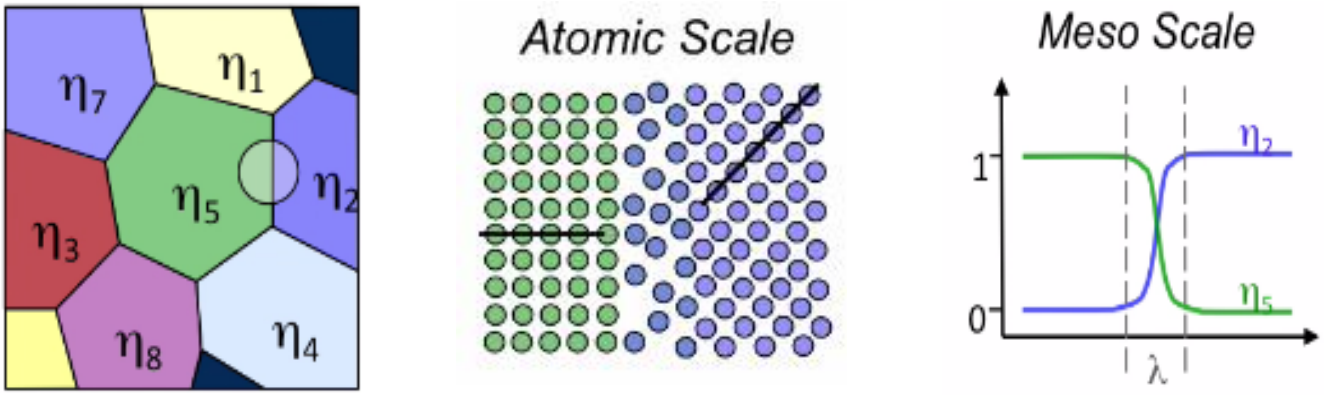

(a) (b) (c)

Figure 13. Different orientation at atomistic scale (b) is represented with different order parameters (a). The order parameters values smoothly transition between zero to 1 value at interface. So, the interface is diffused instead of sharp.

F is the total free energy. The negative sign in the Allen-Cahn equation represents that the order parameters evolve to minimize the total Gibbs free energy of the system. The total the free energy is represented using the following equation:

$$F = \int (f_{bulk} + f_{interface}) dv.$$

So, the total free energy consists of bulk or chemical free energy density, f_{bulk}, and interface free energy density, $f_{interface}$,. All the energies are summed up in to the total free energy, F.

Heat Equation:

In this work, we coupled the phase field method with heat conduction. We added thermal spikes in the system by explicitly representing the heat generation in the heat equation:

$$\rho C_P \frac{\partial T}{\partial t} - \nabla.(k\nabla T) = \dot{q},$$

where $\frac{\partial T}{\partial t}$ is the rate of change of temperature, k is the thermal conductivity, $\dot{q}$ is the volumetric heat generation term, ρ is the mass density, and C_p is the specific heat capacity. If we divide the equation by ρC_p,

$$\frac{\partial T}{\partial t} - \alpha \nabla^2 T + \frac{\dot{q}}{\rho C_p} = 0,$$

where $\alpha = \frac{k}{\rho C_P}$ is the thermal diffusivity.

MARMOT simulation of isothermal irradiation grain growth

MARMOT is a phase field simulation tool based on the MOOSE finite element software. It is developed under the NEAMS program to predict the microstructure evolution in reactor materials, such as fission gas swelling and release, grain growth, creep, fuel cracking or fracture [12] and the corresponding changes. Mesoscale microstructural simulations are then used to inform the macroscale fuel performance tool like BISON [13].

The coupled grain growth and heat conduction model was implemented in MARMOT; it is fully quantitative, and it requires grain boundary energy, γ_{GB}, the grain boundary mobility prefactor, M_o, and activation energy, Q for a given material. The computational cost of the model in MARMOT has been reduced using the grain tracker algorithm. This advanced algorithm allows us to use a small number of order parameters (8 to 11 for 2D) to model any number of grains, such as 1000 grains. Moreover, MARMOT has the capability in coupling multi physics.

The heat generation of the thermal spikes is defined using existing capability in MOOSE. It is defined by the magnitude of the heat source during a spike $\dot{q}$, the average rate at which the spikes occur $\dot{s}$ in units of spikes per second per unit volume (a function of the fluence), the radius of the area over which the heat is applied d_{spike}, and the length of time over which the heat source is maintained (hold time, t_{hold}). The values for these quantities were set to mimic the ion irradiation conditions used in the in-situ experiments. The values used for the model are shown in Table 2.

Table 2:

Parameter Name	Value
Thermal Spike Radius, d_{spike}	$9.57 - 9.79\ nm$
Hold Time (t_{hold})	1×10^{-12} to $1 \times 10^{-10}\ s$
Average thermal spike energy, Q	24.8 to 26.5 KeV
Thermal Spike Generated per ion per nm, χ	0.03837 to 0.04263 $\frac{\text{spikes}}{\text{ion nm}}$
Ion Flux	$6.25 \times 10^{12}\ \frac{ions}{cm^2 * s}$
Initial Grain Size	3 to 4 nm
Incident Ion energy/type	Kr 1 MeV
Fluence	16 to 1120 KC $\left(1KC\ =\ 6.3 \times 10^{16}\ \frac{ions}{m^2}\right)$
Thermal Conductivity, k	2 to 4 $\frac{W}{m-k}$

Molar heat capacity, C_o	$192.56 \text{ to } 235.35 \frac{J}{mol\ k}$
$Specific\ heat, C_p$	$0.713 \text{ to } 0.872 \frac{J}{g\ k}$
UO_2 molar mass	0.27 kg/mol
UO_2 density, ρ	$10.97 \times 10^3 \frac{kg}{m^3}$
Grain Boundary Energy, γ_{GB}	$1.56 \text{ to } 5.87 \times 10^{-4} T \pm 0.3\ \frac{J}{m^2}$
Grain Boundary Mobility, M_{GB}	$M_o \exp\left(-\frac{E_a}{RT}\right)$
Activation Energy, E_a	3 eV
Mobility Prefactor, M_o	$2.14 \pm 0.15 \times 10^{-7}\ \frac{m^4}{Js}$

The value used for the thermal diffusivity was

$$\alpha = \frac{K\left(\frac{W}{m\,k}\right)}{\rho\left(\frac{kg}{m^3}\right) C_p\left(\frac{J}{kg\,k}\right)} = \frac{3}{10.97 \times 10^3 \times 0.7925 \times 10^{-3}} = 0.345 \frac{m^2}{s}$$

The magnitude of the heat generated by each thermal spike

$$\dot{q} = \frac{Q}{V \times hold\ time} = \frac{Q}{\frac{4}{3}\pi r^3 (hold\ time)}$$

$$= \frac{25.65 \times 10^3 eV}{\frac{4}{3}\pi (4.84)^3\ nm^3 \times 10^{-11}\ s} = 5.4 \times 10^{12} \frac{eV}{nm^3 s}$$

where Q is the average thermal spike energy. Then,

$$\frac{\dot{q}}{\rho C_p} = \frac{5.4 * 10^{12}\left(\frac{eV}{nm^3 * s}\right)}{10.97 * 10^3\left(\frac{kg}{m^3}\right) * 0.7925 * 10^{-3}\left(\frac{J}{kg - k}\right)} = 9.95 \times 10^{13} \frac{K}{s}$$

The average rate at which the spikes occur $\dot{s}$ is defined as

$$\dot{s} = ion\ flux\ \left(\frac{ion}{cm^2\ s}\right) \times \frac{\frac{thermal\ spike}{ion}}{thickness\ (nm)}$$

$$\dot{s} = 6.25 \times 10^{12}\ \frac{ion}{cm^2\ s} \times \frac{1}{10^{14}\ \frac{nm^2}{cm^2}} \times 0.0405\ \frac{\text{spikes}}{\text{ion nm}}$$

$$\dot{s} = 0.00253\ \frac{spikes}{nm^3 s} = 2.52 * 10^{-12}\ \frac{spikes}{nm^3\ ns}$$

If we consider 100 initial grains with an initial average grain size of 3 nm, the domain size will be approximately 30 nm by 30 nm in 2D. The experimentally found initial grain size was 3 to 4 nm. In our simulation, we assume an average grain size of 5 nm by choosing the domain size of 50 nm by 50 nm. This is due to the fact that, we need to choose a larger interfacial thickness of 2 nm compared to the realistic case because of the abrupt change in temperature due to thermal spike events. The choice of having larger interface thickness will facilitate the convergence issue as we have more elements across the interface.

Simulation results of heat conduction only: [Input File 1]

Instead of an isothermal domain (constant temperature, T over the domain), we incorporate T as a coupled variable. Each unit of time in the simulations is equal to 100 ns. However, in the simulations no significant events happen in between thermal spikes. Thus, to accelerate the simulations, we increased the thermal spike rate by 5 orders of magnitude to force the thermal spikes closer together, making each unit of time in the simulations equivalent to 0.01 s. The temperature is fixed at 300 K at the boundary, to represent the thermal sink surrounding the irradiated sample. The results just solving the heat equation are shown in *Figure 14*. Each time a spike event occurs, the temperature abruptly rose as high as 10,000K then maintained that temperature during the hold time, before going back to room (300K).

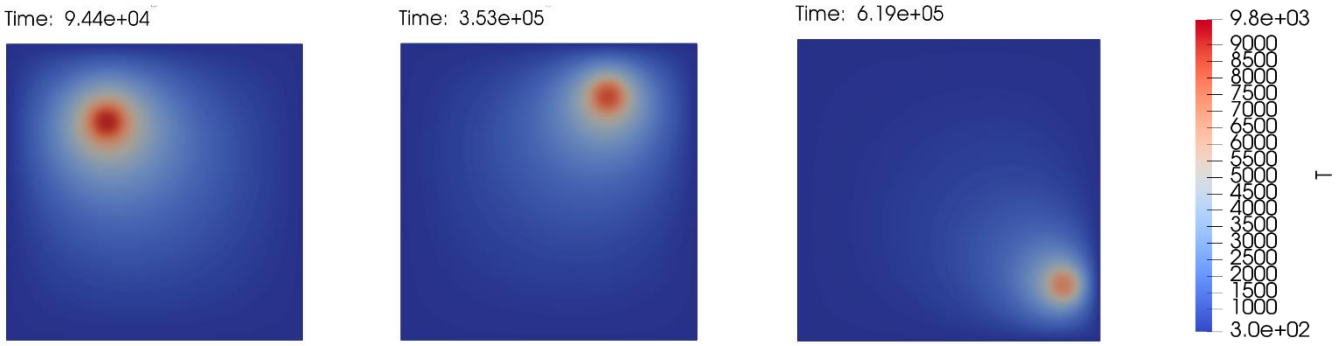

Figure 14. Simulation results with just heat conduction, where thermal spikes occur at random times and locations within the domain. The temperature profile is shown at three times: (a) 9.44×10^4 simulation time units, or 944 s; (b) 3.53×10^5 simulation time units, or 3,530 s; (c) 6.19×10^5 simulation time units, or 6,190 s.

Simulation results of Grain growth only: [Input File 2 and 3]

As a benchmark case, before simulating the grain growth under ion irradiation, we simulated grain growth at 300 K without irradiation. As we can in *Figure 15* at room temperature (300K) without irradiation, no grain growth occurred. This is consistent with the observed behavior in room temperature experiments. Each unit of simulation time was equal to 100 ns.

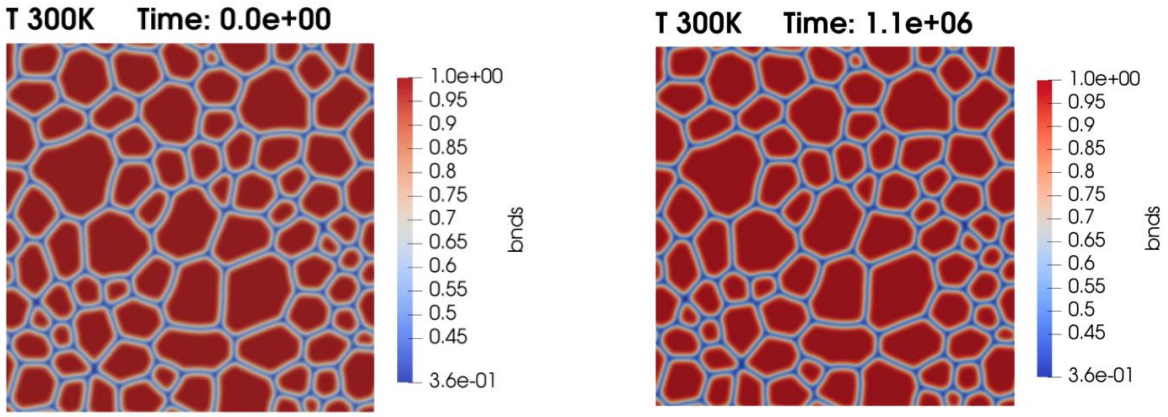

(a) (b)

Figure 15. Grain growth at room temperature (300K). The initial grain structure (a) and the grain structure after 0.11 s (b) are identical.

Coupling of Heat Conduction with Thermal Spikes with Grain Growth [Input file 2 and 4]

When we couple the heat conduction model with thermal spikes with the grain growth model, we can see irradiation-enhanced grain growth at 300K. The simulation time is the same as used with just heat conduction, such that one unit of simulation time is equal to 0.01 s. The final grain structure after ion irradiation for 5,400 s are shown in Fig. 9. The initial grain structure is the same as shown in *Figure 15*(a). The final grain structure without irradiation is also shown, for comparison.

Under irradiation, a large amount of grain boundary migration occurs due to the ion irradiation, even though no thermal grain growth occurred at the same temperature. Large amount of grain growth occurs in the center of the domain, but not at the outer regions. This is due to the fixed 300 K temperature at the boundaries, such that the large temperatures were not experienced near the boundaries of the domain. The change in the number of grains over time is shown in Fig. 7(c). Grains disappear very quickly at the beginning of irradiation, but as the average grain size increases the grains disappear at a decreasing rate.

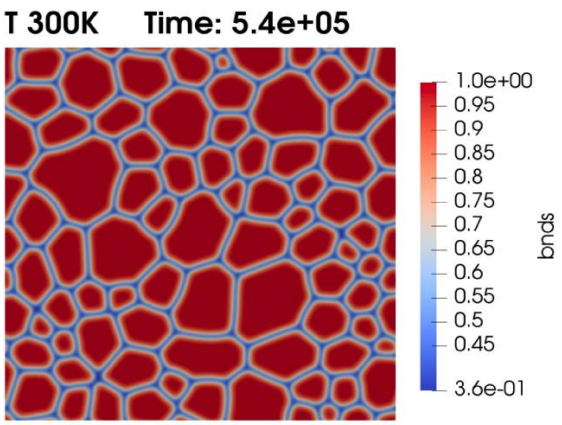

(a)

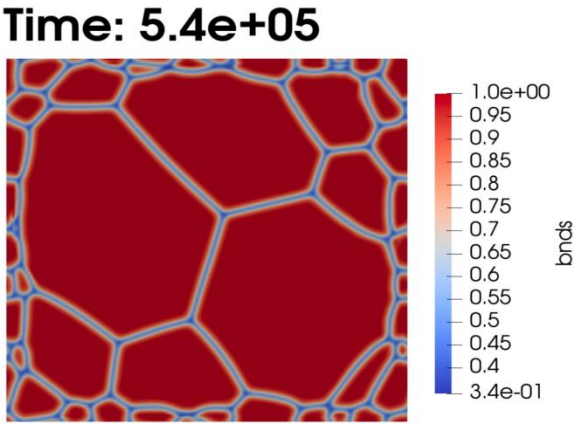

(b)

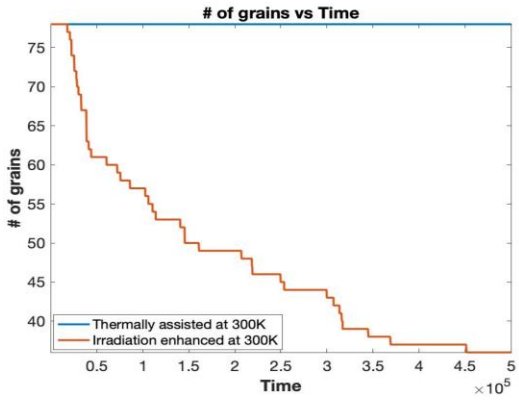

(c)

Figure 16. Grain growth at room temperature (300 K) with thermal spikes from ion irradiation. (a) The final grain structure without irradiation (same as 6(b)); (b) The final grain structure with thermal spikes from ion irradiation. The initial microstructure was same for both (Figure 6(a)); (c) decrease in the number of grains over time.